Journal of Nanoparticle Research (2006) 8: 79–97
DOI 10.1007/s11051-005-8024-2

Optical properties of zinc oxide nano-particles embedded in dielectric medium for UV region: Numerical simulation

S.M. Al-Hilli* and M. Willander
*Physical Electronics and Photonics, Department of Physics, Göteborg University, SE-41296, Göteborg, Sweden; *Author for correspondence (E-mail: salhilli@fy.chalmers.se)*

Received 30 March 2005; accepted in revised form 22 May 2005

Key words: ZnO nanoparticle, optical properties, DDA method, hexagonal ZnO, modelling and simulation

Abstract

Zinc oxide nano-particles have been used by cosmetic industry for many years because they are extensively used as agents to attenuate (absorb and/or scatter) the ultraviolet radiation. In the most UV-attenuating agent is formulated in which the metal oxide nano-particles are incorporated into liquid media or polymer media are manufactured, such as sunscreens and skin care cosmetics. In this paper we study the wavelength dependence on the particle size ($r_{\text{eff}} = 10$–100 nm) by solving the scattering problem of hexagonal ZnO particle for different shapes (plate, equal ratio, column) using the discrete dipole approximation method to find the absorption, scattering, and extinction efficiencies for the UV region (30–400 nm). A new modified hexagonal shape is introduced to determine the scattering problem and it is assumed in this study that the wavelength is comparable to the particle size. From these results, we conclude that the optimum particle radius to block the UV radiation is between $r_{\text{eff}} = 40$–80 nm.

Introduction

Zinc Oxide nano-particles have attracted much interest because of various remarkable physical and chemical properties distinctive from conventional bulk materials. ZnO has a hexagonal wurtzite structure (space group C6 mc) with lattice constants of $a = 3.250$ Å and $c = 5.207$ Å, a direct band gap of 3.37 eV (368 nm) and large exciton binding energy of 60 meV at room temperature (Dulub et al., 2002; Meyer & Marx, 2003). Due to the radial quantum confinement effect, ZnO nano-particles possess high density of states at the band edge.

Scientists have proven that ultraviolet A (UVA) radiation is a major culprit in photo-aging and skin cancers (Fairhurst & Mitchnick, 1997). Unfortunately, most sunscreens don't protect against long-wave UVA. Ultraviolet radiation that reaches the earth and damages skin can be divided into three key wavelengths (Fairhurst & Mitchnick, 1997): (1) Short-wave UVA (32–280 nm) or UVC, (2) UVB (280–320 nm), and (3) Long-wave UVA (320–400 nm) or UVA. UVB which primarily reaches the top-most layer of skin is thought to be responsible for acute photo-damage, including sunburn and some non-melanoma skin cancers and recently found that kind of radiation can kill some kinds of skin cancers. UVA rays which penetrate deep into skin, are responsible for elastic tissue damage and photo-aging, and are thought to be important in causing more aggressive skin cancers, including deadly melanomas. Inorganic UV absorbers (ZnO) have many desirable characteristics such as a long history of topical use, low irritancy, broad spectrum absorption and high photo-stability. Because of

these characteristics zinc oxide has long recognized for its medicinal properties as an anti-irritant and astringent as well as its UV blocking properties, in sunscreens (Shore, 1990).

The purpose of this study is to characterize the influence of the particle shape (hexagonal), and size (plate, equal ratio, column) on the optical properties (scattering, absorption, and extinction efficiencies) for moderate size diameter ($D = 20$–200 nm), comparable to the optically incident radiation that dominant particle size range in sunscreens. The general framework for modelling the optical response of a collection of spheres, which make the hexagonal shape, involves a self-consistent solution of the response of each particle to the incident field and the scattered fields of the other particles by adopting the 'discrete dipole approximation' method (DDA method). We also investigate the effect of particle size at the UV region (30–400 nm). We seek to answer the following question: what is the effective diameter of these hexagonal nano-particles to protect the skin from the UVA, UVB, and UVC regions?

It is desired to have a high transparency for visible light and to attenuate the UV radiation effectively with lower content of zinc oxide particles, and this nano-meter size of primary single particles must be dispersed homogeneously into the medium. This study is a necessary and essential first step toward realistic modelling to determine extinction, absorption, scattering efficiencies for hexagonal shape ZnO nano-particles of the various sizes in the UV spectra having dimensions comparable to the wavelength of incident radiation.

Numerical method (DDA scattering method)

The DDA has been applied to compute scattering and absorption by targets of size comparable to the wavelength in a broad range of problems.

Scattering problem

To describe light scattering from an arbitrarily shaped nano-particle, we have adopted approach method known as the DDA, as first formulated by Purcell and Pennypacker (Purcell & Pennypacker, 1973), is a highly efficient and flexible technique for studying scattering and absorption of electromagnetic radiation in non-spherical particle shapes (Draine, 1998). One main shortcoming of the DDA is that it takes account of only pair dipole–dipole interactions between particles (or point dipoles). This is due to the special form of the zero-point-interaction Green function included in the general formulation of the theory (Markel et al., 1996; Draine, 1998). In this method, the particle of interest (hexagonal) is divided into a cubic array of N-point dipoles with polarizabilities denoted as α_i (and no higher multipole polarizabilities), and centres at position r_i. The interaction of each dipole with a local electric field E_{loc} (here we have neglected the magnetic dipole radiation) will induce a polarization given by (omitting frequency factors $e^{i\omega t}$):

$$P_i = \alpha_i \cdot E_{\mathrm{loc}}(r_i) \tag{1}$$

E_{loc}, for isolated particles, is the sum of the incident field and the field, E_{dip}, from all other dipoles in the particle,

$$E_{\mathrm{loc}}(r_i) = E_{\mathrm{loc},i} = E_{\mathrm{inc},i} + E_{\mathrm{dip},i} = E_{\mathrm{o}} e^{(ik\cdot r_i)} - \sum_{j\neq i} A_{ij} \cdot P_j \tag{2}$$

where E_{o} and k are the amplitude and the wave vector of the incident wave, respectively. The interaction matrix A has the form:

$$A_{ij} \cdot P_j = \frac{e^{(ikr_{ij})}}{r_{ij}^3}\left\{k^2 r_{ij} \times \left(r_{ij} \times P_j\right) + \frac{\left(1 - ikr_{ij}\right)}{r_{ij}^2} \times \left[r_{ij}^2 P_j - 3r_{ij}\left(r_{ij} \cdot P_j\right)\right]\right\}, \quad (j \neq i) \tag{3}$$

where $k = 2\pi/\lambda$ is the wave number, λ is the wavelength of incident light, and $r_{ij} = | r_i - r_j |$ is the vector between the ith and jth dipoles. Substituting Eq. (2) and (3) into Eq. (1) and rearranging terms, we generate an equation of the form:

$$\left(\alpha^{-1}\right) P_i + \sum_{j\neq i} A_{ij} \cdot P_j = E_{\mathrm{inc},i} \text{ or } A' \cdot P = E_{\mathrm{inc}} \tag{4}$$

where A_{ij} is the matrix of coefficients in Eq. (3). In the form of Eq. (4) P and E_{inc} are $3N$ vectors and A' is a $3N \times 3N$ symmetric matrix constructed from the 3×3 interparticle interaction matrices A_{ij} with additional terms α_i^{-1} along the diagonal

($A_{ii} = \alpha_i^{-1}$). Solving this set of $3N$ complex linear equations allows the polarization vector P to be obtained, and consequently the optical properties to be calculated. The complex linear Eq. (4) for the induced polarizations were solved using DD SCAT6.1 program written by Draine and Flatau (Draine & Flatau, 2004a). We have modified their code to generate hexagonal particle geometry with different size.

Solution method (complex-conjugate gradient method (CCG method)

Rather than direct methods for solving Eq. (4), CCG methods for finding P iteratively have proven to be effective and efficient (Press et al., 1986; Peterson et al., 1991). The CCG algorithm used to solve Eq. (4) described by Petravic and Kuo (Petravic & Kuo-Petravic, 1979). In brief, beginning from an initial guess $P_i^{(0)}$, the CCG method generates a sequence $P_i^{(n)}$ where ($n = 1,2,...$) that converges monotonically for estimate P until Eq. (4) is solved to some error criterion. The error tolerance may be specified as:

$$\frac{|A^+AP - A^+E|}{|A^+E|} < h, \tag{5}$$

where A^+ is the Hermitian conjugate of A (i.e., $(A^+)_{ij} \equiv (A_{ji})^*$), and h is the error tolerance. We typically use $h = 10^{-5}$ in order to satisfy Eq. (4) to high accuracy.

The number of iterations required to obtain an accurate solution depends upon the grain shape, N, the refractive index, (kr_{eff}), and the initial starting point. In this study we fellow Flatau (Flatau, 1997) in using the stabilized version of Bi-Conjugate Gradients (Bi-CGSTAB) method (Van der Vosrt, 1992) with preconditioning. For more details about the algorithms see references (Van der Vosrt, 1992; de Cunha & Hopkins, 1995).

Target generation (geometry or the shape of the particle)

Each dipole may be thought of as representing the polarizability of a particular subvolume of target material and these dipoles are located on a periodic cubic lattice.

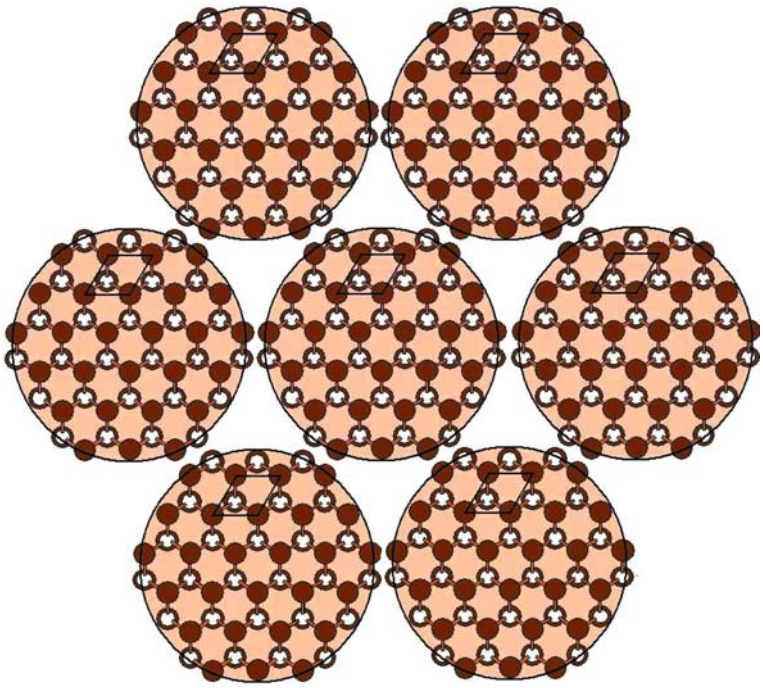

Figure 1. Hexagonal sphere – packing of the building block of the ZnO model (plane view).

There is some arbitrariness in the construction of the array of point dipoles intended to represent a solid target of specified geometry. To construct a target of volume V in the 'Target Frame' (TF) we use the following algorithm to generate the dipole array and we restrict ourselves to cubic lattices (Draine, 2000).

1. We assume that the target orientation is fixed relative to a coordinate system $\hat{x}, \hat{y}, \hat{z}$.
2. Let the target centroid define the origin of coordinates.
3. Choose a trial lattice spacing d and construct a lattice $(x,y,z) = (n_x,n_y,n_z)d + (o_x,o_y,o_z)d$, where the n_i are integers and the offset vector (o_x,o_y,o_z), allows the target centroid to be located at a lattice point or between lattice points, as appropriate.
4. Having chosen d and (o_x,o_y,o_z), the target array are now taken to consist of the lattice points located within the target volume; let N be the number of such points.
5. With these N lattice points now determined, we make a small adjustment to the lattice spacing and set $d = (V/N)^{1/3}$ (when N is large, the d so obtained is nearly the same as the original trial d because each dipole represents a volume d^3 of material, we require the array volume $Nd^3 = V$).
6. For each occupied site i where $(i = 1,...,N)$ assign a dipole polarizability α_i. It is convenient to characterize the target size by the effective radius:

$$r_{\text{eff}} \equiv \left(\frac{3V}{4\pi}\right)^{1/3} = \left(\frac{3N}{4\pi}\right)^{1/3} d \tag{6}$$

   r_{eff} is simply the radius of a sphere of equal volume.

Beside the above steps if we want to consider three-dimensional hexagonal shape of identical spheres from the generator matrix for the lattice vectors must follow these steps (Conway & Sloane, 1999):

1. The overall hexagonal shape of a particle is defined by the positions of the dipole spheres which have unit diameter.
2. We built the suitable lattice packing that has the properties that $(0, 0, 0)$ is a center and that if there are spheres with centers u and ν then there are also spheres with centers $u + \nu$ and $u - \nu$. This set of centers forms an additive group (in crystallography these lattices are usually called Bravais lattices).
3. We can find three centers ν_1, ν_2, ν_3 (or in general n centers ν_1, ν_2, ν_3, ..., ν_n) such that the set of all centers consists of the sums $\sum k_i \nu_i$ where the k_i are integers.
4. The vectors $\nu_1,\ldots,\nu_n$ are then called a basis for the lattice, and the parallelotope is consisting of the points: $\tau_1 \nu_1 + \cdots + \tau_n \nu_n$ where $(0 \leq \tau_i < 1)$.
5. Let the coordinates of the basis vectors be:

$$\begin{aligned} v_1 &= (v_{11}, v_{12}, \ldots, v_{1m}), \\ v_2 &= (v_{21}, v_{22}, \ldots, v_{2m}), \\ &\cdots\cdots \\ &\cdots\cdots \\ v_n &= (v_{n1}, v_{n2}, \ldots, v_{nm}), \end{aligned}$$

   where $m \geq n$. (Sometimes it is convenient to use $m > n$ coordinates to describe an n-dimensional lattice.)
6. The matrix:

$$M = \begin{bmatrix} v_{11} & v_{12} & \cdots & v_{1m} \\ v_{21} & v_{22} & \cdots & v_{2m} \\ \cdots & \cdots & \cdots & \cdots \\ v_{n1} & v_{n2} & \cdots & v_{nm} \end{bmatrix}$$

   is called a generator matrix for the lattice, and the lattice vectors consist of all the vectors: ξM, where $\xi = (\xi_1,...,\xi_n)$ is an arbitrary vector with integer components ξ_i.
7. In our case we first generate planar hexagonal lattice by using M as a square matrix:

$$M = \begin{bmatrix} 1 & 0 \\ 1/2 & \sqrt{3}/2 \end{bmatrix},$$

8. Then to generate three-dimensional hexagonal shapes in a fundamental region by extending the planar hexagonal lattice as a building block for the first layer to any vertex–vertex diameter of the hexagonal face and repeated this layer many times fills the whole space of the final three-dimensional hexagonal particle. The planer hexagonal building block is pictured in Figure 1.

Dipole polarizabilities

Since DDA results depend directly upon the dipole polarizabilities, it is important to deter-

mine the optimal method for choosing such polarizabilities. Draine and Goodman (Draine & Goodman, 1993) established the 'lattice dispersion relation' (LDR) method for prescribing the dipole polarizabilities. They solved a closely related problem, choosing the dipole polarizabilities such that an infinite lattice of point dipoles will propagate electromagnetic plane waves with the same dispersion relation as a medium of specified dielectric function ε. The unique aspect of this prescription is that it depends not only on refractive index m but also on the direction of propagation and the polarization state of the incident radiation.

$$\alpha^{\mathrm{LDR}} = \frac{\alpha^{(0)}}{1+\left(\frac{\alpha^{(0)}}{d^3}\right)\left[(b_1+m^2b_2+m^2b_3S)(kd)^2-\left(\frac{2}{3}\right)i(kd)^3\right]}, \tag{7}$$

where $\alpha^{(0)}=\alpha^{(\mathrm{CMR})}$ is the 'Clausius–Mossotti Relation' (CMR) polarizability in the infinite wavelength limit of the DDA, $kd \rightarrow 0$ (Jackson,

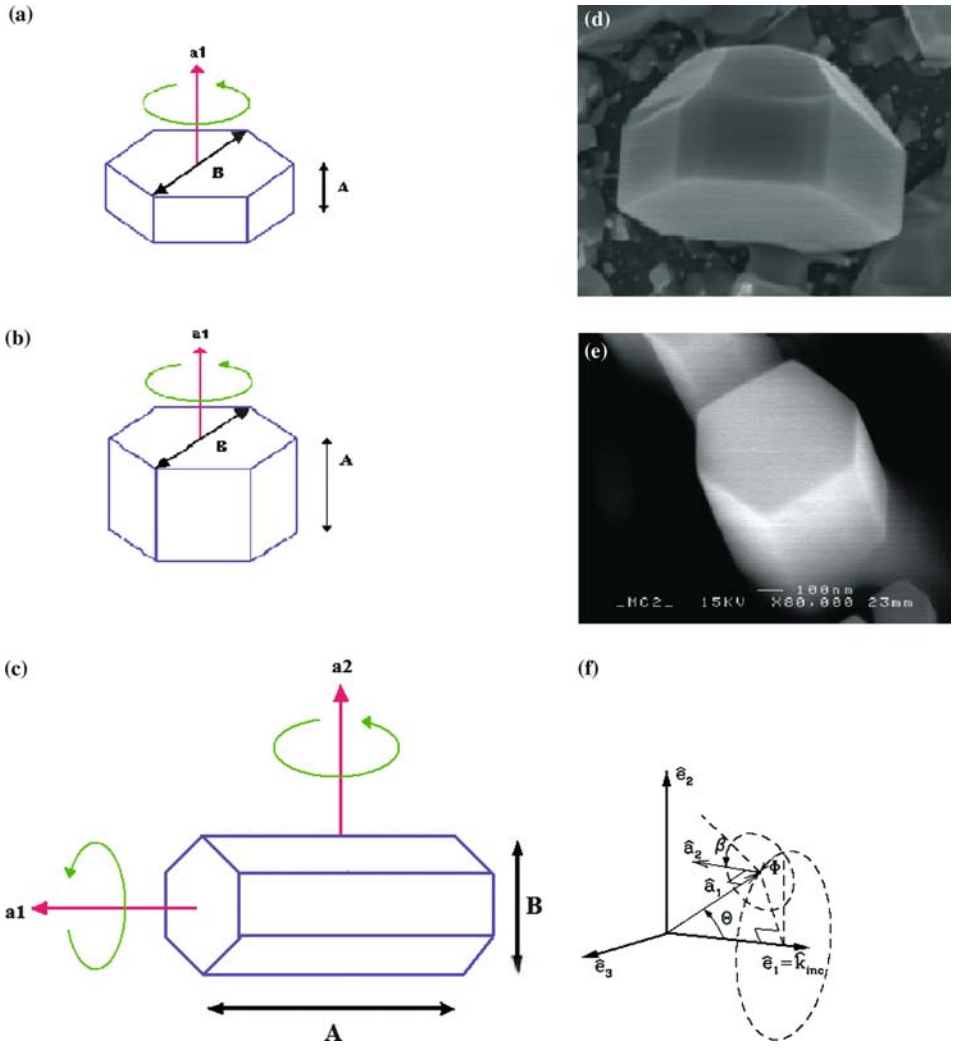

Figure 2. Hexagonal particle shapes (a) plate, (b) equal ratio, (c) column, (d) real plate hexagonal ZnO particle (Ref. (Klason P. et al., Submitted)), (e) real column hexagonal ZnO particle (Ref. (Klason P. et al., Submitted)), and (f) target frame orientation (Ref. Draine & Flatau, 2004b).

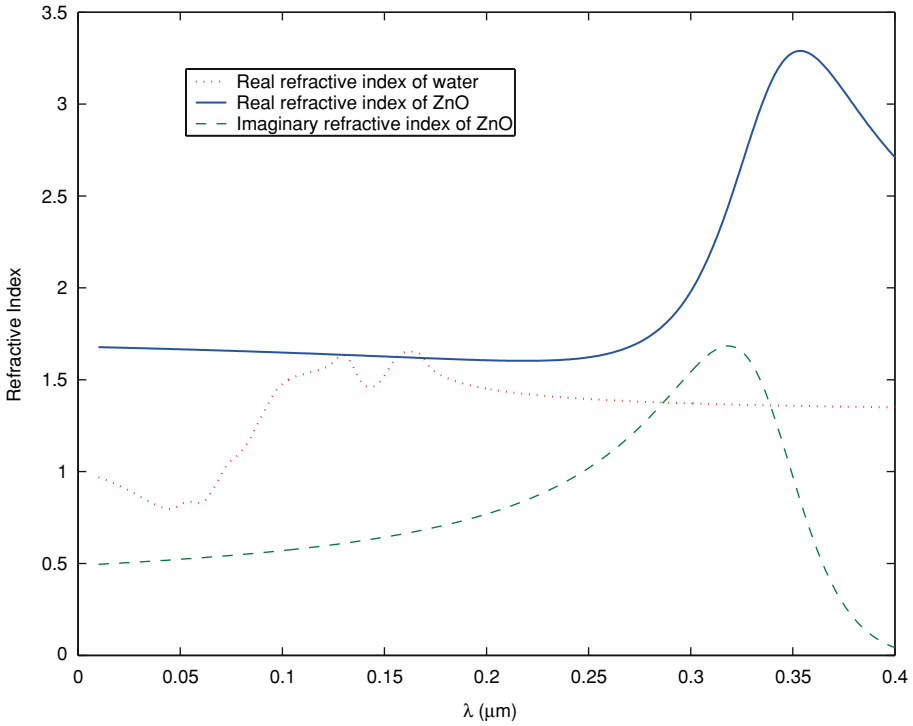

Figure 3. Complex refractive index of ZnO and real part refractive index of water *versus* wavelength.

1975), which is given as a function of the (complex) refractive index m:

$$\alpha^{(\mathrm{CMR})} = \left(\frac{3d^3}{4\pi}\right)\left(\frac{\varepsilon - 1}{\varepsilon + 2}\right) = \left(\frac{3d^3}{4\pi}\right)\left(\frac{m^2 - 1}{m^2 + 2}\right), \tag{8}$$

$b_1 = -1.8915316$, $b_2 = 0.1648469$, $b_3 = -1.7700004$, and S is a function of the propagation direction and polarization of the incident wave. S is given as:

$$S = \sum_i (a_i e_i)^2 \tag{9}$$

where a and e are the unit propagation and polarization vectors, respectively.

In this 'lattice dispersion relation' (LDR) approach, the radiation-reaction correction emerges naturally, and the polarizability is given (to order $(kd)^3$). In our study we adopt this LDR polarizability.

Validity criteria

The constraints for the validity of the DDA code are:

1. All coordinates are defined in terms of the distance between neighbouring dipoles d, which is given by $d = (4\pi/3)^{1/3}\ R$ (for example, if two particles have radii 10 nm, then the distance between the dipoles is 16.12 nm).The lattice spacing (inter-dipole separation) d to be small enough compared with the wavelength λ of light in the surrounding target medium, $\rho = kd|m| < 1$, where ρ is the wave phase shift, $k = 2\pi\ /\lambda$ is the wave number, λ is the wavelength in surrounding medium and m is the complex index of refraction. However, if accurate calculations of the scattering phase function are desired, a more conservative criterion $kd|m| \leq\ 0.5$ is needed.
2. d must be small enough to describe the target particle shape satisfactorily (any structural lengths in the target).
3. The technique is not well suited for targets with very large complex refractive index m, it works well for materials with $|m| \leq 2$ and target dimension $D \leq 5\lambda$. Otherwise the error in polarization is too large in the surface monolayer of the particle (Draine & Flatau, 1994).

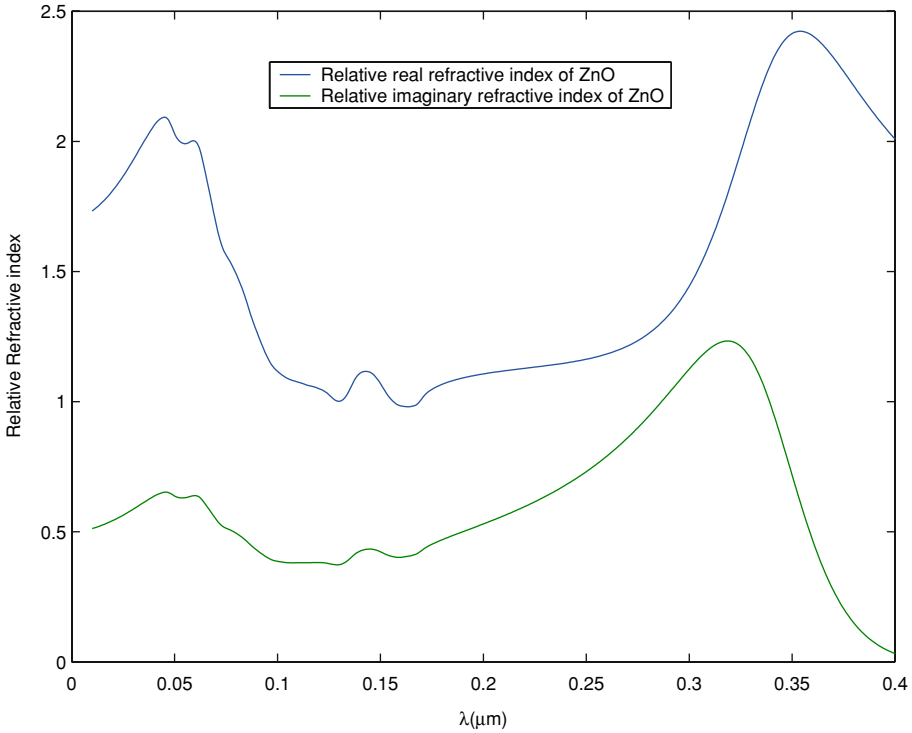

Figure 4. Complex refractive index of ZnO in medium *versus* the wavelength.

4. The typical number of dipoles needed to obtain a reliable computational result using the DDA code can be determined by calculating the minimum number of dipoles needed per particle. When a particle is represented by a 3-dimensional array of N dipoles, its volume is Nd^3, which be equal to $4\pi\ R^3/3$,

$$N = \frac{4\pi}{3}\left(\frac{R}{d}\right)^3 = \frac{4\pi}{3}\left(\frac{2\pi R|m|}{\rho\lambda}\right)^3 \approx 1039\left(\frac{R|m|}{\rho\lambda}\right)^3 \tag{10}$$

since d is related to the wave phase shift ρ by $d = \rho/(k|m|)$ (Xing & Hanner, 1997; Draine, 2000).

Target orientation

In the DDSCAT6.1 code, the particle orientation specified relative to the incident wave by letting the axes $\hat{a}_1$,$\hat{a}_2$ (with $\hat{a}_1 \cdot \hat{a}_2 = 0$), and $\hat{a}_3 = \hat{a}_1 \times \hat{a}_2$ are the principal axes of the target. The particle orientation is completely specified by the orientations of any two nonparallel fixed axes, in particular $\hat{a}_1$ and $\hat{a}_2$ also DDSCAT6.1 code define a 'Scattering Frame' (SF) which defined by unit vectors $\hat{e}_1 = \hat{k}$,$\hat{e}_2 \perp \hat{e}_1$ and $\hat{e}_3 = \hat{e}_1 \times \hat{e}_2$. Three angles are required to specify the target orientation. The orientation of $\hat{a}_1$ in the scattering frame is described by the two angles $\Theta \in [0, \pi]$ defines the angle between incident wave and target axis, and $\Phi \in [0, 2\pi]$ gives the rotation of target axis around k. A third angle $\beta \in [0,2\pi]$ describes rotations of the target axis $\hat{a}_2$ around $\hat{a}_1$. Detailed information is given in the User Guide for the Discrete Dipole Approximation Code DDSCAT 6.1 (Draine & Flatau, 2004b). In our study we specify $\beta = 0$, $\Phi = 0$, and $\Theta = 0°$, 60°, 90° see Figure 2 for our case.

Incident polarization state

The incident radiation is always assumed to propagate along the x-axis in the 'Lab Frame' (LF). The DDSCAT6.1 code specifies incident polarization state $\hat{e}_{01}$ to be along the y-axis and consequently polarization state $\hat{e}_{02}$ will automatically be taken to be along the z-axis. We choose unpolarized incident light for our study.

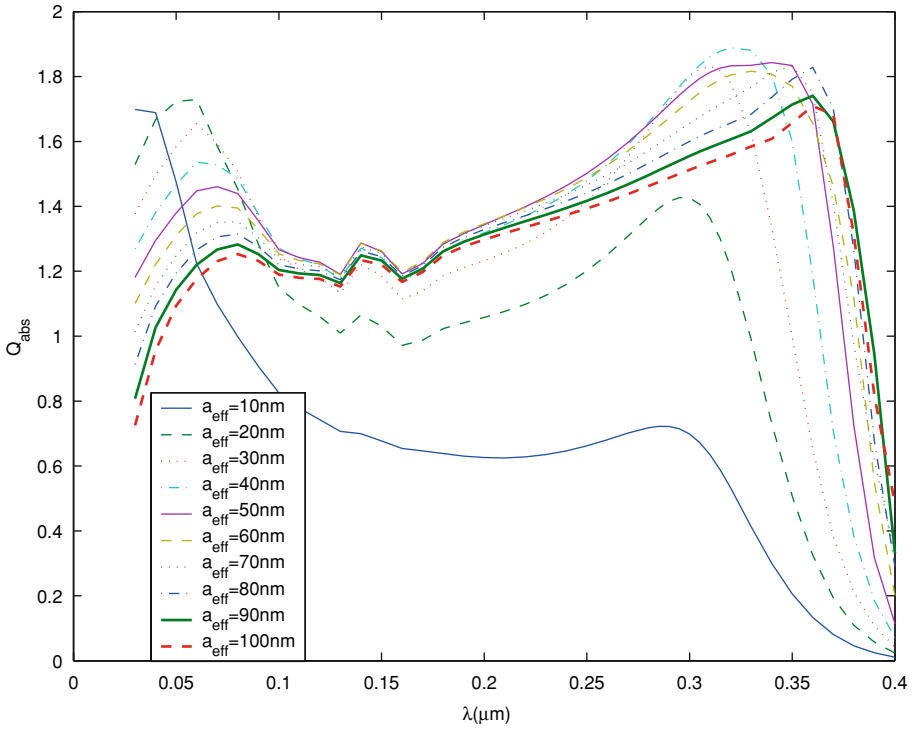

Figure 5. Absorption efficiency factor *versus* wavelength for plate-like hexagonal ZnO particle with different effective radius.

Scattering directions

The scattering direction is specified through angles θ_s and ϕ_s. The scattering angle θ_s is simply the angle between the incident beam (along direction $\hat{x}$) and the scattered beam ($\theta_s = 0$ for forward scattering, $\theta_s = 180°$ for backscattering).

The scattering angle ϕ_s specifies the orientation of the 'scattering plane' relative to the $(\hat{x} - \hat{y})$ plane in the Lab Frame. When $\phi_s = 0$ the scattering plane is assumed to coincide with $(\hat{x} - \hat{y})$ plane. When $\phi_s = 90°$ the scattering plane is assumed to coincide with $(\hat{x} - \hat{z})$ plane. Within the scattering directions are specified by $(0 \leq \theta_s \leq 180°)$. In our case we specify $\phi_s = 0, 90°$ for $\theta_s = 10°(10°)180°$.

Optical properties using DDA method

Optical cross-sections

DDA solves the problem of scattering and absorption by an array of polarizable point dipoles interacting with a monochromatic plane wave incident from infinity. Once the polarizations, P_i, are known, the extinction C_{ext}, absorption C_{abs}, and scattering C_{sca} cross sections may be evaluated from the optical theorem, thus giving (Van de Hulst, 1957):

$$C_{ext} = \frac{4\pi k}{|E_o|^2} \sum_{i=1}^{N} \mathrm{Im}\left(E^*_{loc,i} \cdot P_i\right) \tag{11}$$

$$C_{abs} = \frac{4\pi k}{|E_o|^2} \sum_{i=1}^{N} \left\{ \mathrm{Im}\left[P_i \cdot \left(\alpha_i^{-1}\right)^* P_i^*\right] - \frac{2}{3} k^3 P_i \cdot P_i^* \right\} \tag{12}$$

The scattering cross section can in principle be obtained from the difference of the extinction and absorption cross sections:

$$C_{sca} = C_{ext} - C_{abs} \tag{13}$$

When absorption is dominant, this requires that C_{ext} and C_{abs} be computed to high accuracy. Since the method of computation is iterative, it may be costly to obtain the solution vectors P_i to the necessary degree of accuracy. It is possible to compute the scattering cross section directly by

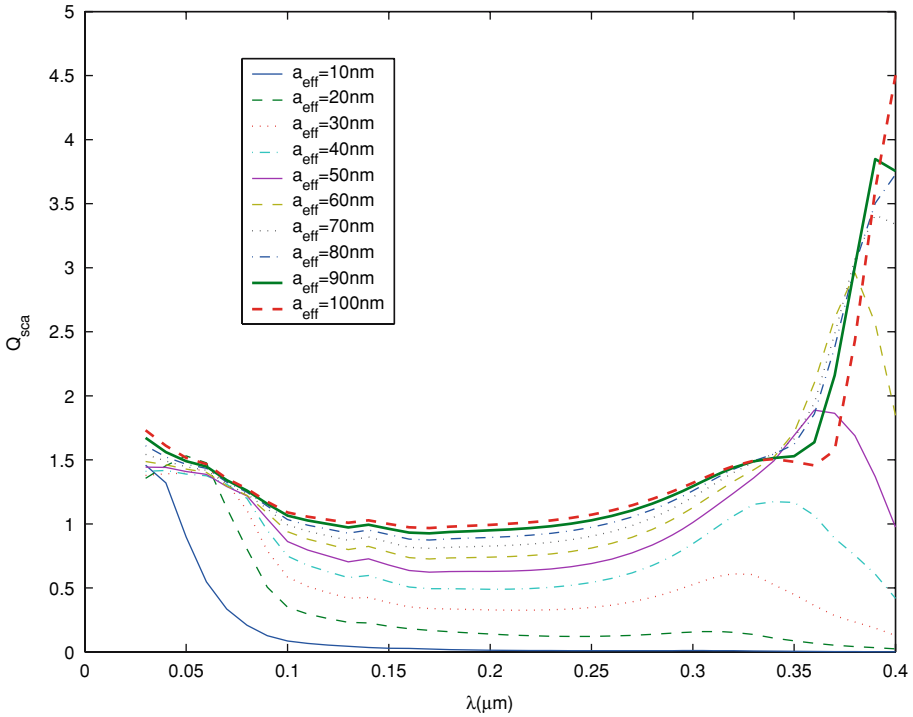

Figure 6. Scattering efficiency factor *versus* wavelength for plate-like hexagonal ZnO particle with different effective radius.

computing the power radiated by the array of oscillating dipoles:

$$C_{\text{sca}} = \frac{k^4}{|E_{\text{inc}}|^2} \int d\Omega \left| \sum_{i=1}^{N} [P_i - \hat{n}(\hat{n} \cdot P_i)] \exp(-ik\hat{n} \cdot r_i) \right|^2 \tag{14}$$

where $\hat{n}$ is a unit vector in the direction, and $d\Omega$ is the element of solid angle. And the following quantities can be calculated after we get the optical cross-sections:

1. Absorption efficiency factor $Q_{\text{abs}} = C_{\text{abs}}/\pi r_{\text{eff}}^2$.
2. Scattering efficiency factor $Q_{\text{sca}} = C_{\text{sca}}/\pi r_{\text{eff}}^2$.
3. Extinction efficiency factor $Q_{\text{ext}} = Q_{\text{sca}} + Q_{\text{abs}}$.

Application to targets embedded in dielectric media

For many applications of interest the target body is embedded in a (non-absorbing) dielectric medium with (real) dielectric function $\varepsilon_{\text{target}}(\omega)$, or (real) refractive index $m_{\text{target}}(\omega) = \sqrt{\varepsilon_{\text{target}}}$. DDA is fully applicable to these scattering problems, except that:

1. The dielectric function or refractive index supplied to DDA should be the relative dielectric function:

$$\varepsilon(\omega) = \frac{\varepsilon_{\text{target}}(\omega)}{\varepsilon_{\text{medium}}(\omega)}$$ or relative refractive index:

$$m(\omega) = \frac{m_{\text{target}}(\omega)}{m_{\text{medium}}(\omega)}. \tag{15}$$

2. The wavelength λ specified in DDA should be the wavelength in the medium:

$$\lambda = \frac{\lambda_{\text{vac}}}{m_{\text{medium}}}, \tag{16}$$

where $\lambda_{\text{vac}} = 2\pi c/\omega$ is the wavelength *in vacuo*.

The absorption, scattering and extinction efficiency factors calculated by DDA will then be equal to the physical cross sections for absorption, scattering, and extinction divided by $\pi\, r_{\text{eff}}^2$ (e.g., the attenuation coefficient for radiation propagating

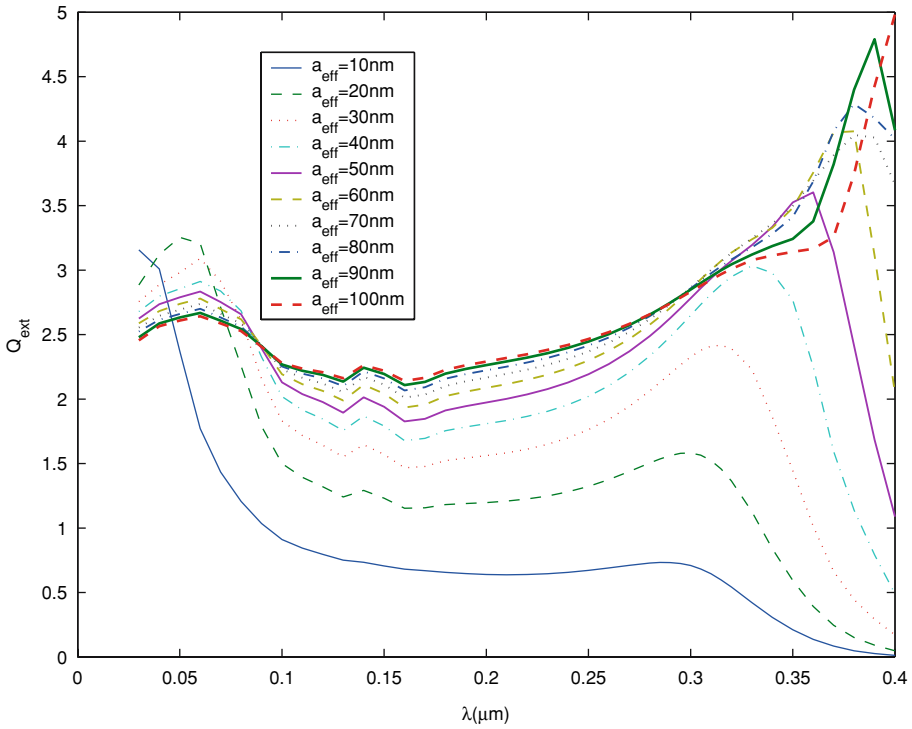

Figure 7. Extinction efficiency factor *versus* wavelength for plate-like hexagonal ZnO particle with different effective radius.

through a medium with a density n_t of scatterers will be just $\alpha = n_t Q_{ext} \pi r_{\text{eff}}^2$).

Relative refractive index of ZnO in UV region

The refractive index is important parameter which governs the intensity of scattered light. The parameter here is the relative refractive index, which is the ratio between the refractive index of the particles (ZnO) and that to the matrix, such as the oil phase (in our study we take it water for simplicity).

Simulating the refractive index data of the Zinc oxide

Due to the lack of real optical measurements to ZnO nano-particles in the UV region, we simulate the data for real and imaginary parts of refractive index by adopting the works by Dakhel (Dakhel, 2003) as approximate data. Dakhel calculate the spectral extinction coefficient $k(\lambda)$ of the Zinc oxide film of thickness (173 nm) in the fundamental absorption band gap by utilizing two equations. The first is Fresnel equation (Borns & Wolf, 1980; Heavens, 1991; Dakhel, 2001), and the second is Swanepoel equation (Swanepoel, 1983) for transmittance $T(\lambda)$ at strong absorption coefficient α. The curve of $k(\lambda)$ is obtained from the best-fit with the numerical solution points of the above mentioned two equations by introducing the experimental $T(\lambda)$ values (This method is referred to as the T-method). The extinction coefficient as a function of energy $k(E)$ in the interband region that calculated by T-method can be fitted to the four parameters Forouhi–Bloomer (FB) equation (Forouhi & Bloomer, 1991):

$$k(E) = A\frac{(E - E_{\text{FB}})^2}{E^2 - B \cdot E + C} \quad \text{for } E > E_{\text{FB}} \qquad (17)$$

where $E_{\text{FB}}\,(\text{eV}) = 2.9$, $A = 0.49$, $B\,(\text{eV}) = 7.21$, $C\,(\text{eV})^2 = 13.2$, $E_{\text{g}}\,(\text{eV}) = 3.28$, $E_{\text{m}}\,(\text{eV}) = 3.51$ (is the energy value at which n has its maximum value).

This model works very well in the short-wavelength side of each curve, where the interband

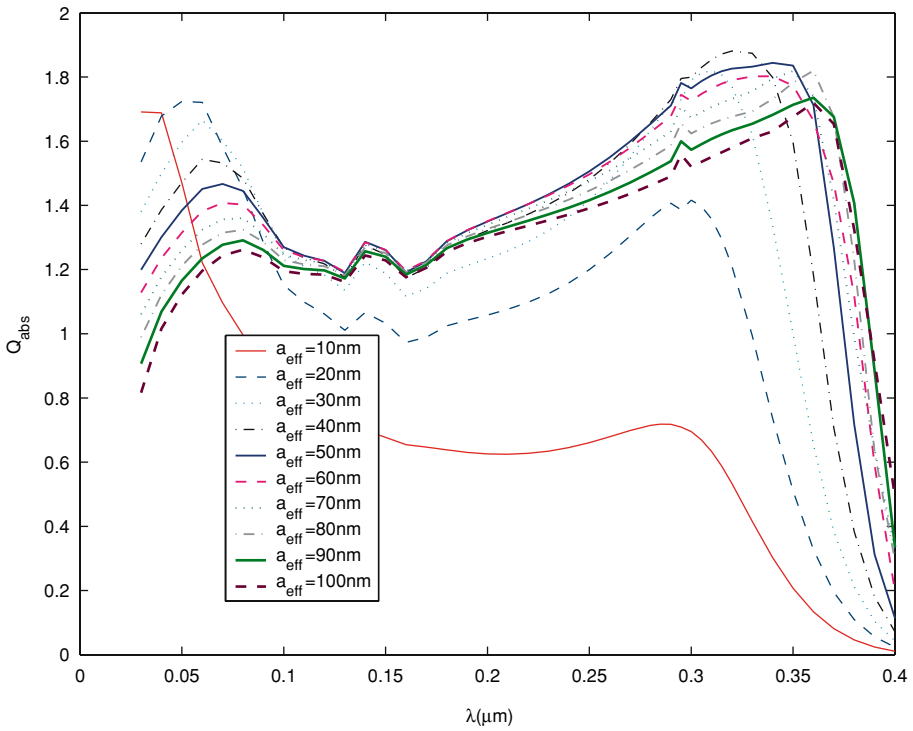

Figure 8. Absorption efficiency factor *versus* wavelength for equal ratio hexagonal ZnO particle with different effective radius.

transitions dominate the spectrum. The above fitting parameters can determine the spectral values of refractive index $n(E)$ according to 'Kramers–Kronig' (KK) relation (Forouhi & Bloomer, 1991; Kim, 1996):

$$n(E) = n_\infty + \frac{B_p E + C_p}{E^2 - B \cdot E + C} \tag{18}$$

where B_p and C_p are parameters given by:

$$B_P = \left(\frac{A}{B}\right)\left(2C - B^2 + 2E_{FB}B - 2E_{FB}^2\right)$$

$$C_P = \left(\frac{A}{D}\right)\left[B\left(C + E_{FB}^2\right) - 4E_{FB}C\right]$$

$$D = \left(4C - B^2\right)^{\frac{1}{2}}$$

where $n_\infty(\lambda) = 1.68$ (is a matching parameter whose value is chosen to appropriate the ellipsometric value of n at 632.8 nm wavelength). Figure 3 shows the real and imaginary parts of refractive index of ZnO *versus* the wavelength in vacuo for UV region according to Eqs. (17) and (18).

The real refractive index data of the dielectric medium (water)

We adopt Segelstein (Segelstein, 1981) data for the real refractive index data of water in the UV region and put it in interpolation program to get all the values wanted for our calculation. Figure 3 shows the water real part of refractive index.

Relative refractive index

We calculate the relative complex refractive index (the ratio of refractive index of the ZnO nano-particles to water real refractive index) using Eq. (15). Now the only data needed to calculate is the wavelength in the medium and we get it by applying the Eq. (16). With this step we get the data needed to run the code DDSCAT6.1 for our study on optical properties of ZnO nano-particles. Figure 4 shows the relative ZnO complex refractive index versus the wavelength in the medium.

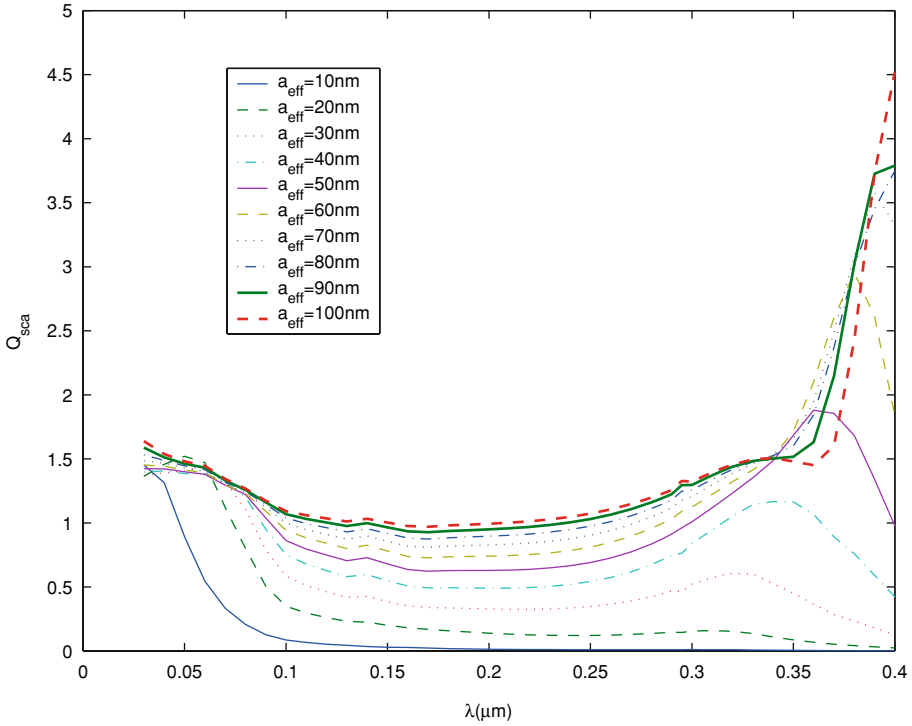

Figure 9. Scattering efficiency factor *versus* wavelength for equal ratio hexagonal ZnO particle with different effective radius.

Results

We start by analyzing the optical properties of individual ZnO hexagonal particles of a given shapes (plate, equal ratio, column) and different sizes by means of DDA method described in the section Numerical method (DDA scattering method). The analysis of mono-disperse particles helps to examine the relative importance of different shapes as a function of size and wavelength. In addition, some particle size distributions might be rather narrow. In this case, optical properties calculated for a specific particle size well approximate those of polydisperse particles with a narrow size distribution.

The applicability and accuracy of the DDA was estimated by comparing the DDA solutions with those from the Mie theory for a compact sphere with the same total dipole moment (Draine & Goodman, 1993; Draine & Flatau, 1994). Draine and Flatau concluded that the extinction and scattering sections can be computed to accuracies of a few percent provided that $|m|kd < 0.5$ and $N > 10^5$ are used. In this study the shape of the hexagonal particles is characterized by the aspect ratio defined by (A/B) where A denotes the length and B denotes the width of the hexagonal particle as sketched in Figure 2. Three different particle shapes are considered in this study: hexagonal plates with aspect ratio (0.49), hexagonal particles with aspect ratio (1.000), and hexagonal columns with aspect ratio (1.5098). The selection of aspect ratios in this study is done to represent nature reasonably well (see Figure 2d,e for real picture of ZnO hexagonal nano-particles taken from reference (Klason P. et al., Submitted)). The values of the size range $r_{\text{eff}} = 10$ nm(10 nm)100 nm for all the three hexagonal particle shapes. Also we emphasis our study to the behaviour of the wavelength dependence of extinction, absorption, and scattering efficiencies for the three ranges in UV region [UVC: $\lambda = 30$ nm (10 nm)280 nm, UVB: $\lambda = 280$ nm(5 nm)320 nm, and UVA: $\lambda = 320$ nm(10 nm)400 nm].

In order to model the most continuous surface of the particle as possible we chose to set the distance between dipoles to the smallest value between $d = 0.03$ nm and 0.0014 nm depending on

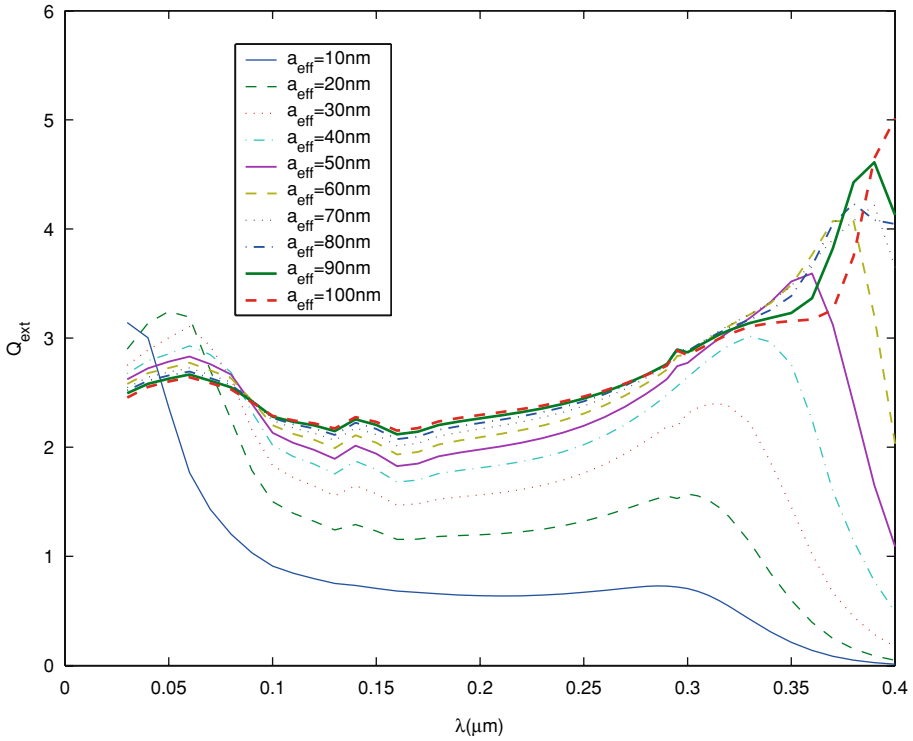

Figure 10. Extinction efficiency factor versus wavelength for equal ratio hexagonal ZnO particle with different effective radius.

the effective radius of the particle. Consequently, the number of dipoles on the surface is large; this high density helps to remove the effect of artificial granularity due to the DDA approximation in the density function. The interdipole spacing d, used in performing the DDA calculations, should verify the criterion:$d/\lambda_{\text{metal}} \approx 10^{-4}$.

Hexagonal plate-like

In this section, the plate-like hexagonal particle with aspect ratio = 0.491–0.52 for (2-D) orientation [assumed the hexagonal particle are oriented randomly on a horizontal plane, i.e., with their major axis in the horizontal plane]. The a_1 and a_2 axis are fixed in the target frame. The longest dimension of the particle is taken to be parallel to the horizontal plane, the a_2 axis lies in the horizontal plane and the a_1 axis is taken to be parallel to the propagation direction of the incident radiation (Figure 2a). Two different numbers of dipoles are considered here ($N = 6097$ and 48,775), where N-face = 469 and N-layer = 13 for the first N, N-face = 1951 N-layer = 25 for the second N.

Absorption, scattering, and extinction efficiencies

Figures 5, 6, and 7 show the absorption, scattering, and extinction efficiency factors *versus* wavelengths for single hexagonal nano-particle, respectively. Figure 5 exhibits two broad peaks, the first one have maximum at $\lambda = 30$ nm with high intensity for the $r_{\text{eff}} = 10$ nm and the second peak have maximum at $\lambda = 250$ nm with less intensity and much broader than the first. The value of absorption efficiency for the range from $\lambda = 130$ nm to $\lambda = 250$ nm approximately constant, and the value of Q_{abs} after the second peak reduced to minimum. With increasing the effective radius of the particle (increasing the size) the shape of the first peak will get much broader with low intensity and shifted toward long wavelengths, and for the second peak will be less broadening with increasing the intensity until we get the maximum at $r_{\text{eff}} = 40$ nm and this peak get low reduction in intensity and a shift of the peak toward long

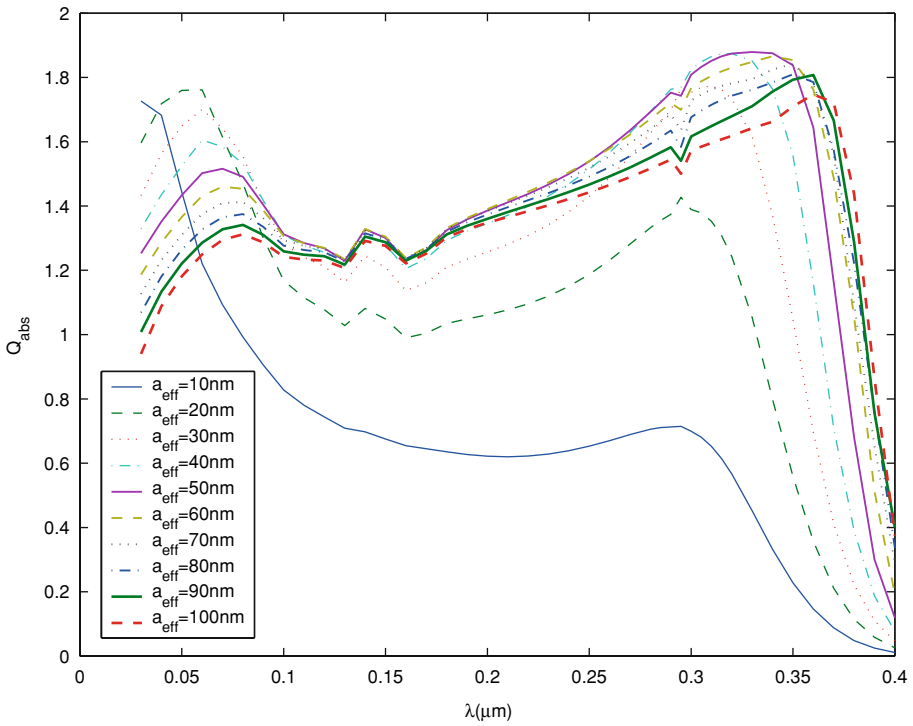

Figure 11. Absorption efficiency factor *versus* wavelength for column hexagonal ZnO particle with different effective radius.

wavelengths, with rapid reduction in intensity toward minimum for all particle sizes.

In Figure 6 exhibit two small broad peaks for $r_{\text{eff}} = 10$ nm, the first have maximum at $\lambda = 30$ nm with rapid reduction to the minimum values for Q_{sca} and continue with approximate constant value with increasing the wavelengths. By increasing the size of the particle the first peak will shifted toward the long wavelengths and continue with broad reduction in intensity to reach a constant value until the second broad peak appear, the intensity get increased, the broadening reduced and maximum value shifted toward long wavelengths.

Figure 7 exhibit two peaks for $r_{\text{eff}} = 10$ nm, the first peak have maximum value at $\lambda = 30$ nm with rapid reduction in intensity to reach approximately constant value until the second broad small peak reached, which have maximum at $\lambda = 290$ nm and continue to reduce in intensity after the second peak to reach the minimum value at $\lambda = 400$ nm. By increasing the particle size, the first peak get more broadening and shifted toward long wavelengths and continue to reduced after the first peak to reach approximate constant value and this value increased with increasing the particle size. The second peak intensity get increased with reduction in the broadening and shifted toward long wavelengths by increasing the particle size.

Hexagonal particle with equal ratio

The equal lengths hexagonal particle with aspect ratio = 1.000 is investigated. Two different numbers of dipoles are considered here [$N = 11{,}725$ with (N-face = 469 and N-layer = 25) and $N = 99{,}501$ with (N-face = 1951 and N-layer = 51)]. The a_2 axis lies in the horizontal plane and the a_1 axis is taken to be parallel to the propagation direction of the incident radiation (Figure 2b).

Absorption, scattering, and extinction efficiencies

Figures (8, 9, and 10) show the absorption, scattering, and extinction efficiency factors *versus* wavelengths for single hexagonal nano-particle, respectively.

The behaviours of the efficiencies are just like in the plate-like hexagonal particle except for the

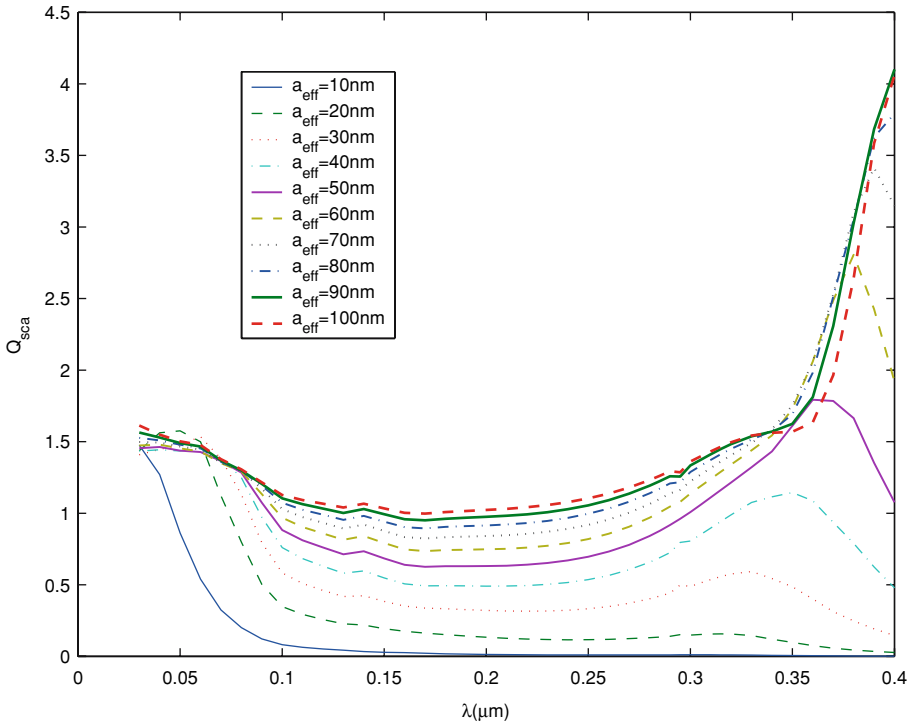

Figure 12. Scattering efficiency factor *versus* wavelength for column hexagonal ZnO particle with different effective radius.

intensity of these efficiencies and the maximum values of the shifted two peaks.

Hexagonal column

The hexagonal column with aspect ratio = 1.509–1.56 is considered. The propagation direction of the incident wave is taken to be parallel to the axis a_2 and the axis a_1 always lies in a horizontal plane (Figure 2c). Two different numbers of dipoles are considered here [N = 18,291 with (N-face = 469 and N-layer = 39) and N = 150,227 with (N-face = 1951 and N-layer = 77)].

Absorption, scattering, and extinction efficiencies

Figures 11, 12, and 13 show the absorption, scattering, and extinction efficiency factors *versus* wavelengths for single hexagonal nano-particle, respectively.

The behaviours of the efficiencies are just like in the plate-like hexagonal particle except for the intensity of these efficiencies and the maximum values of the shifted two peaks.

Discussion

The location and the intensity of the first and second peaks in the Figures 5–13, which shifted are dependent on the wavelength and particle size. To explain this case, the first peak in the UVC region arises from the dipole excitations and the relation between the polarizability and dielectric function to extract ε (ω) (Wood & Ashcroft, 1982) and the second peak in the UVA associated with the band gap at (380 nm) for the bulk ZnO and this peak is shifted to the shorter wavelengths as the particle size decreased because the wavelength dependence of the absorption cross section seems to depend on the mean optical thickness of the hexagonal nano-particle which is function of the N and λ (Kozasa et al., 1992).

The comparisons between absorption and scattering efficiency factors for ZnO particles for three hexagonal shapes with same effective radius are shown in Figures 14 and 15), the results for effective radius = 40 and 80 nm. For each size, both figures display two bands of similar posi-

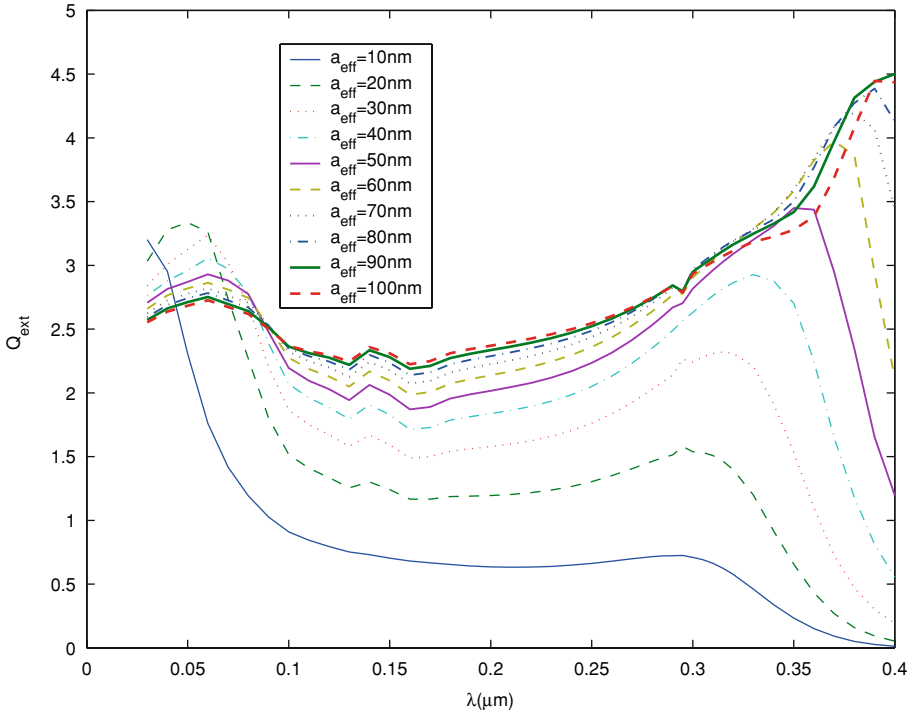

Figure 13. Extinction efficiency factor *versus* wavelength for column hexagonal ZnO particle with different effective radius.

tion, intensity and shape for the plate and equal lengths hexagonal particles with small difference between the values for the column shape. The similarity between the plate and equal lengths hexagonal particles came from aspect ratio assumed for the plate (0.49), this value get less effective with decreasing the effective radius as we can see from the curves of effective radius 40 nm, we found it much similar and have the same values in most regions than the curves of 80 nm. And the difference in intensity between the plate and column hexagonal particles arises obviously from the difference of the target frame axes a_1 and a_2 of the plate and column hexagonal ZnO particle and of course from the different in shape of plate and column.

When the particle size increases, its shape being kept constant, the only increase the peak intensity, which, in this case, is proportional to the hexagonal volume. Conversely, DDA appears in agreement with the expected physical behaviour by predicting a broadening and a shift of the peaks in addition to the intensity increase. The DDA method takes into account the multipolar interactions and retardation affects, therefore, the DDA method, which was found to be in good agreement for ZnO hexagonal particles and appears as the easiest satisfactory method for our purpose.

Conclusion

In this work, we have developed a model, based upon light scattering by single particle, which enables us to account satisfactorily for the absorption, scattering, and extinction spectra of hexagonal ZnO particles.

The method used to obtain the hexagonal shape differs from those given up in DDA shape for hexagonal prism and presents some advantages in provides the size and shape of the hexagonal particles and give good results of optical properties.

We performed the simulations over a three shapes of ZnO hexagonal particles and we obtained absorption, scattering, and extinction spectra which always lead to hexagonal aggregate

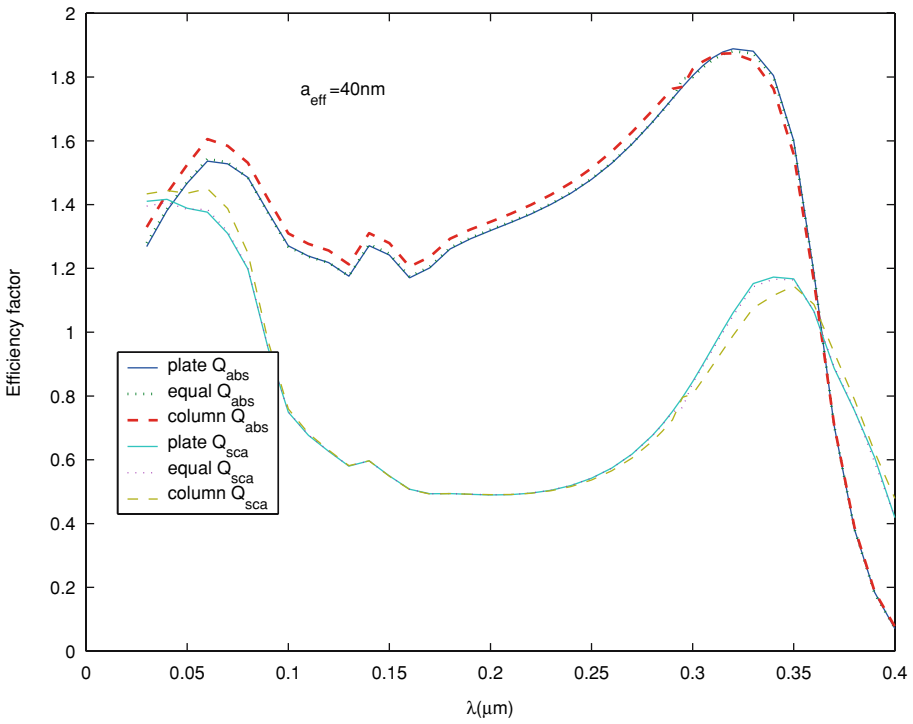

Figure 14. Absorption and scattering efficiency factors *versus* wavelength for plate, equal ratio, and column hexagonal ZnO particle with constant effective radius (40 nm).

distributions very similar in shape and size to the real hexagonal ZnO particles. Besides, the absor ption, scattering, and extinction efficiency spectra of the various targets are quite different from each other; they generally display two narrow bands which maxima are located at different wavelengths for each target.

From the scattering figures, we see the scattering intensity is proportional to the particle diameter. Therefore, it is important to use effective particle radius of ZnO for obtaining minimum scattering and maximum absorption for certain region from the UV regions. Where the band gap absorption (The mechanism of UV absorption in ZnO involves the use of photon energy to excite electrons from the valence band to the conduction band and ZnO have band gap for the corresponding wavelength 380 nm and the light below these wavelengths has sufficient energy to excite electrons, and hence is absorbed by ZnO particles) is primarily a function of the number of atoms in the path of the UV light. Therefore, we found a high improvement in the UV absorption with decreasing particle size.

Finally, the obtained results indicate the main features of the hexagonal particles effect for both the shape and the intensity of the peaks. Anyhow, the results suggest, that hexagonal ZnO particles that display a strong extinction band greatly shifted toward long wavelengths are mainly constituted of spheres small compared with the wavelength. It can then be concluded that the efficiency spectra of the molecules producing the hexagonal particle arise from the excitation of the surface plasmon resonances of these small spherical dipoles.

The next step in such simulations would be to study the optical properties in the visible region and compare these studies with the experimental data of ZnO particles; experiments performed at several scattering angles would bring different band profiles and might confirm the present study. Also we must investigate the influence of the surface roughness in the model.

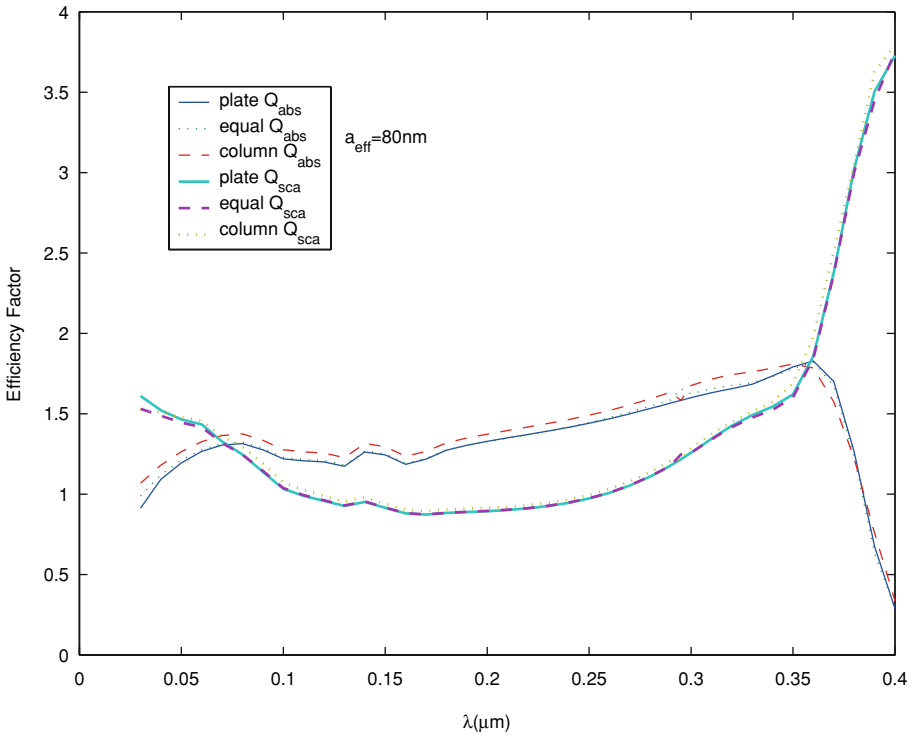

Figure 15. Absorption and scattering efficiency factors *versus* wavelength for plate, equal ratio, and column hexagonal ZnO particle with constant effective radius (80 nm).

References

Borns M. & E. Wolf, 1980. Principle of Optics. Oxford: Pergamon Press.

Conway J.H. & N.J.A. Sloane, 1999. Sphere Packings, Lattices and Group. 3rd edn. Springer-Verlag, New York, Sections 1.2, 1.4, 4.6.1, and 4.6.2.

Dakhel A.A., 2001. Optical constants of evaporated gadolinium oxide, J. Opt. A: Pure Appl. Opt. 3, 452–454.

Dakhel A.A., 2003. Structure, refractive index dispersion and optical absorption properties of evaporated Zn–Eu oxide films, Mater. Chem. Phys. 81, 56–62.

de Cunha R.D. & T. Hopkins, 1995. The Parallel Iterative Methods (PIM) package for the solution of systems of linear equations on parallel computers, Appl. Num. Maths. 19, 33–50.

Draine B.T., 1998. The discrete-dipole approximation and its application to interstellar graphite grains, Astrophys. J. 333, 848–872.

Dranie B.T., 2000. The discrete-dipole approximation for light scattering by irregular targets. In: Mishchenko M.I., Hovenier J.W., & Travis L.D. eds. Light scattering by Nonspherical Particles: Theroy, Measurements, and Geophysical Applications. Academic Press, N.Y., pp. 131–145.

Draine B.T., 2004a. Princeton University Observatory, Princeton NJ, 08544–1001 and Flatau P.J., University of California, San Diego, Scripps Institution of Oceanography, La Jolla, California 92093–0221, USA. Program DDSCAT6.1.

Draine B.T. & P.J. Flatau, 2004b. User Guide for the Discrete Dipole Approximation Code DDSCAT.6.1. http://arxiv.org/abs/astro-ph/xxx.

Draine B.T. & P.J. Flatau, 1994. The discrete dipole approximation for scattering calculations, J. Opt. Soc. Am. A 11, 1491–1499.

Draine B.T. & J. Goodman, 1993. Beyond Clausius-Mossotti: Wave propagation on a polarizable point lattice and the discrete dipole approximation, Astrophys. J. 405, 685–697.

Dulub O., L.A. Boatner & U. Diebold, 2002. STM study of the geometric and electronic structure of ZnO(0001)-Zn, (0001′)-O, (101′0), and (112′0) surfaces, Surf. Sci. 519, 201–217.

Fairhurst D. & M.A. Mitchnick, 1997. In: Lowe N.J., Shaath N.A. and Pathak M.A. eds. Sunscreens; Development, Evaluation, and Regulatory Aspects. 2nd edn. Marcel Dekker, New York, p. 313.

Flatau P.J., 1997. Improvements in the discrete-dipole approximation method of computing scattering and absorption, Opt. Lett. 22, 1205–1207.

Forouhi A.R. & I. Bloomer, 1991. In: E.D. Palik, ed. Handbook of Optical Constants of Solids II, Calculation of optical constants n and k in the interband region. Academic Press, New York, Chapter 7, pp. 151–175.

Heavens O.S., 1991. Optical Properties of Thin Film. New York: Dover.

Jackson J.D. 1975. Classical Electrodynamics. Wiley, New York, Ch. 4.5, p.152.

Kim S.Y., 1996. Simultaneous determination of refractive index, extinction coefficient, and void distribution of titanium dioxide thin film by optical methods, Appl. Opt. 35, 6703–6707.

Kozasa T., J. Blum & T. Mukai, 1992. Optical properties of dust aggregates: I. Wavelength dependence, Astron. Astrophys. 263, 423–432.

Markel V.A., V.A. Shalaev, E.B. Stechel, W. Kim & R. Armstrong, 1996. Small-particle composites I. Linear optical properties, Phys. Rev. B 53, 2425–2436.

Meyer B. & D. Marx, 2003. Density-functional study of the structure and stability of ZnO surfaces. Phys. Rev. B67, 035403.

Peterson A.F., S.L. Ray, C.H. Chan, and R. Mittra, 1991. In: Sarkar T.K., ed. Application of Conjugate Gradient Method of Electromagnetics and Signal Analysis, Numerical implementation of the conjugate gradient method and the CG-FFT for electromagnetic scattering. Elsevier, New York, Ch. 5.

Petravic M. & G. Kuo-Petravic, 1979. An ILUCG algorithm which minimizes in the euclidean norm, J. Computational Phys. 32, 263–269.

Press W.H., B.P. Flannery, S.A. Teukolsky & W.T. Vetterling,. 1986. Numerical Recipes. Cambridge: Cambridge University Press.

Purcell E.M. & C.R. Pennypacker, 1973. Scattering and absorption of light by nonspherical dielectric grains, Ap. J. 186, 705–714.

Segelstein D., 1981. The Complex Refractive Index of Water. M.Sc. thesis, University of Missouri, Kansas city, USA.

Shore R.E., 1990. Overview of radiation-induced skin cancer in humans, Int J. Radi. Biol. 57, 809–827.

Swanepoel R., 1983. J. Phys. D: Appl. Phys. 10, 1214.

Van de Hulst H.C., 1957. Light scattering by small particles. Wiley, New York, Section 4.21.

Van der Vosrt H.A., 1992. Bi-CGSTAB: A fast and smoothly converging variant of Bi-CG for the solution of nonsymmetric linear systems, SIAM J. Sci. Statist. Comput. 13, 631–644.

Wood D.M. & N.W. Ashcroft, 1982. Quantum size effect in the optical properties of small metallic particles, Phys. Rev. B 25, 6255–6274.

Xing Z. & M.S. Hanner, 1997. Light scattering by aggregate particles, Astron. Astrophys. 324, 805–820.